# Ionic colloidal crystals: Ordered, multicomponent structures via controlled heterocoagulation

Garry R. Maskaly,[1,2] R. Edwin García,[1,3] W. Craig Carter,[1] and Yet-Ming Chiang[1]
[1]*Department of Materials Science and Engineering, Massachusetts Institute of Technology, Cambridge, Massachusetts 02139, USA*
[2]*Physical Chemistry and Applied Spectroscopy, Los Alamos National Laboratory, MS J567, Los Alamos, New Mexico 87544, USA*
[3]*Department of Materials Engineering, Purdue University, West Lafayette, Indiana 47907, USA*
(Received 31 August 2005; published 12 January 2006; publisher error corrected 18 September 2006)

We propose a new type of ordered colloid, the "ionic colloidal crystal" (ICC), which is stabilized by attractive electrostatic interactions analogous to those in atomic ionic materials. The rapid self-organization of colloids via this method should result in a diversity of orderings that are analogous to ionic compounds. Most of these complex structures would be difficult to produce by other methods. We use a Madelung summation approach to evaluate the conditions where ICC's are thermodynamically stable. Using this model, we compare the relative electrostatic energies of various structures showing that the regions of ICC stability are determined by two dimensionless parameters representing charge balance and the spatial extent of the electrostatic interactions. Parallels and distinctions between ICC's and classical ionic crystals are discussed. Monte Carlo simulations are utilized to examine the glass transition and melting temperatures, between which crystallization can occur, of a model system having the rocksalt structure. These tools allow us to make a first-order prediction of the experimentally accessible regions of surface charge, particle size, ionic strength, and temperature where ICC formation is probable.

DOI: 10.1103/PhysRevE.73.011402 PACS number(s): 61.43.Hv

## I. INTRODUCTION

Natural opal's unique optical properties arise from microscopic particles ordering in large arrays. With the availability of monodisperse colloidal particles, extended ordered arrays have been produced artificially through various techniques including hard-sphere interactions, fluid flow, and electrostatic repulsion [1–8]. These arrays are generally composed of a single-particle type, limiting the number of possible structures. To produce a wider variety of structures, various two-component approaches have been implemented [9–17]. The resulting structures are those that occur in metallic systems, such as the $AB$, $AB_2$, and $AB_{13}$ structure types. While some of these structures have ionic analogues (such as CsCl), their stability does not arise from attractive electrostatic forces. These systems exhibit strong variations with the particle volume fraction, the number ratio of the two particles, the size ratios of the two particles, and the degree of size dispersity. This phase space typically has multiple phases present in equilibrium, with one phase often being a colloidal liquidlike phase, where particles have high mobility and can readily rearrange.

In this work, we investigate the possibility of a new type of two-component colloidal crystal that is stabilized by attractive electrostatic interactions. Such attractions are widely considered to only allow random aggregation; however, we show that a mixture of positively and negatively charged particles tailored within certain experimental constraints is energetically and kinetically likely to form an "ionic colloidal crystal" (ICC) [18,19], stabilized by long-range attractive forces. In previous colloidal crystals utilizing repulsive electrostatic interactions, the ordered state minimizes the repulsive energy between many particles in a confined volume; however, in an ICC, the attractive forces involved in crystallization should result in dense ordered aggregates with no need for volumetric confinement. The utilization of controlled attractive interactions makes ICC's a fundamentally new colloidal phenomenon.

A system utilizing attractive forces should allow rapid crystallization while also allowing a more diverse colloidal phase space through the variation of system parameters that tune the relevant interactions. Being fundamentally enthalpy driven rather than entropy driven, ionic colloidal crystallization is more likely to yield robust equilibrium phases, similar to natural ionic compounds. Structures that could be potentially realized include zincblende, which should exhibit a complete photonic band gap with relatively low refractive index contrasts [20], and rutile, which has potential catalysis and filtration applications due to the presence of ordered structural channels. In this paper, we predict the conditions under which ICC's are energetically stable by developing a model reducible to a pair of dimensionless parameters: a screening ratio ($\Lambda$), characterizing the spatial extent of the electrostatic interaction, and a representative point-charge ratio ($Q$). We discuss the control of heterocoagulation that is necessary to avoid low packing density noncrystalline reaction-limited cluster aggregation (RLCA) and diffusion-limited cluster aggregation (DLCA) [21–23], both of which are more typically observed in colloidal systems where both signs of charge are present. We find the conditions under which ICC's are energetically and kinetically favorable to be restrictive, suggesting that they are unlikely to occur accidentally.

## II. BACKGROUND

Colloidal interactions have been widely studied since the seminal works of Derjaguin and Landau [24] and Verwey and Overbeek [25]. The Poisson-Boltzmann equation, which describes the interactions of solvated ions in the potential field of a charged surface, has been widely used to model and

 

predict a variety of colloidal behavior. Here, we utilize the linearized Poisson-Boltzmann equation [Eq. (1)] to model the electrostatic interactions in ICC systems:

$$\nabla^2\psi \cong \kappa^2\psi - \frac{\rho(x,y,z)}{\varepsilon_0\varepsilon_r}. \quad (1)$$

Here $\psi$ is the electrostatic potential, $\kappa$ is the Debye parameter, $\rho$ is the spatial charge distribution, and $\varepsilon_0\varepsilon_r$ is the permeability of the solvent. The linearized Poisson-Boltzmann equation (PBE) strictly applies only for small electrostatic potentials. In the present work its main strength is that it allows analytical solutions that provide physical insight into the experimental parameter spaces favorable for ICC formation. In cases where the electrostatic potential is large, the analytical solutions obtained herein will be less accurate in terms of predicting phase stability, but still useful for illustrating behavioral trends and identifying regimes in which more detailed models are necessary. While numerical solutions to the nonlinear PBE could be used to obtain more accurate results, we use the less computationally intensive analytical solutions to enable characterization of a large phase space, as shown in the results below. Furthermore, for Monte Carlo or Brownian dynamics simulations, it is necessary to linearize the PBE allowing the superposition of particle interactions, as solving the nonlinear PBE for the potential fields in a many-particle system is computationally prohibitive.

It is also necessary to choose appropriate boundary conditions at the particle surfaces in order to accurately model closely approaching colloids. Consider the two limiting cases of a constant surface potential or a constant surface charge. While the constant surface potential boundary condition has been widely used to model heterocoagulation behavior, exemplified by the theory of Hogg, Healy, and Fuerstenau (HHF) [26], models based on this approximation diverge to an infinite binding energy at contact. In reality, at some point during the approach of two oppositely charged particles, the surface must reach a limiting maximum charge in order to maintain a finite energy. Thus, in dense colloidal suspensions we expect particle surfaces to exhibit constant surface charge behavior. Systems in the heterocoagulation regime exhibiting such behavior have been demonstrated [18].

The choice of a suitable interparticle potential is of course also critical. Three principal potentials exist for treating constant-surface-charge behavior under the linearized Poisson-Boltzmann equation [Eq.(1)]: the Yukawa-type potential (or screened Coulomb potential common to DLVO theory [24,25]), the Ohshima potential [27], and the Wiese-Healy potential [28]. Consider the underlying assumptions for each. An important assumption of the Yukawa-type potential is that the ionic strengths of the particle interior and the solution phase are identical. As there are no assumptions about additional neighboring particles, superposition is possible. This potential is commonly used across a wide range of colloidal conditions to model repulsive interactions. However, this potential has not to our knowledge been used to model behavior in attractive systems, primarily due to the fact that it breaks down at close range if the particle core and the solution differ. However, for systems of *low ionic strength*, particularly for those with nearly identical dielectric constants of the solution and particles, it can be shown that the deviations of the Yukawa-type potential from solutions obtained by numerically solving the linearized Poisson-Boltzmann equation over a periodic structure such as an ICC are small as would be expected from the approximations used in developing the potential [18].

The Ohshima potential improves upon the Yukawa-type potential by adding iterative terms correcting for the dielectric constant and ionic strength of the particle core. It includes the Yukawa-type potential as the first-order term, but adds a series of converging infinite sums for these corrections. However, in making these corrections, a new assumption is made that the two interacting particles are only surrounded by solution. Therefore, in dense colloidal suspensions and particularly at low ionic strengths where multiparticle interactions must be taken into account, this model becomes inaccurate.

The Wiese-Healy model assumes that the ionic strength is large, utilizing the Derjaguin approximation [29] to develop the potential. The Ohshima potential converges to the Wiese-Healy potential at large ionic strengths, but is useful over a much larger range of ionic strengths. Therefore the Wiese-Healy potential carries the same limitations as the Ohshima potential.

While no potential is available that is applicable over all regimes of colloidal behavior, we utilize the Yukawa-type potential in this study since low ionic strengths are necessary to develop the repulsion between next-nearest and farther neighbors essential for structural rearrangement into ordered arrays. A simple thought experiment illustrates this point (Fig. 1). Consider the surface of a disordered aggregate. If potentials are only short ranged, meaning the interaction has a shorter length scale than the particle size, a particle in solution can attach to a dissimilar particle on the heteroaggregate, but the energy of this particle is nearly identical to that of a free dipole having only one particle-particle interaction. In the absence of longer-range repulsion, dissociation of the heteroaggregated dipole must occur to allow particle rearrangement. Therefore, a system with only short-ranged interactions will either form, above a critical temperature, a plasmalike suspension of particles attracted to dissimilar particles or, below the critical temperature, a glass consisting of aggregates with no colloidal mobility. This plasmalike and glassy behavior has been reported in DNA-based systems [30] which have predominantly short-ranged interactions. While tunable "melting" points could be achieved, crystallization was prohibited due to the sharp transition to a glassy state. Note that this behavior is not dependent on the exact physical forces but only on the range of the force relative to the particle sizes.

However, in systems with long-range next-nearest-neighbor repulsive interactions, the binding energy of a particle adhered to the surface can be significantly lower than that of a free dipole. In such systems surface and bulk reorganization are possible at temperatures below that required to break all dipoles. The reorganization necessary for crystallization now becomes possible. For electrostatic interactions, in general a low ionic strength will be required to produce these long-range interactions, allowing us to use the

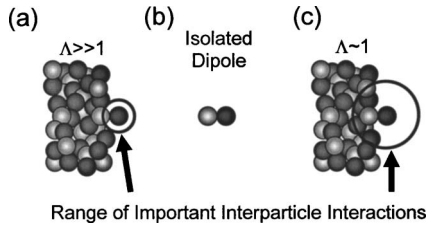


FIG. 1. Three possible environments are considered for a colloidal particle to illustrate the influence of the range of interaction potentials on heterocoagulation behavior. In the first case (a) high ionic strengths lead to large screening and short-range interactions (black circle). This case as drawn is nearly identical in energy to that for an isolated dipole pair (b). The particle in question only interacts significantly with one part. In both of these cases, mobility of the colloids requires a temperature similar to that necessary to make a colloidal "plasma" (where no particles are associated and the aggregate dissociates rather than rearranges). For such a system, only two states may exist: a glassy (frozen state) and a plasmalike state (all free flowing particles). In a system with a low ionic strength (c), the long-range potentials give repulsion between similar particles in the aggregate. The binding energy of a particle to the surface is significantly reduced from that of the dipole state. Here, at a temperature well below the "plasma" temperature, the system can rearrange. This construction illustrates why systems with only short range forces (i.e., van der Waals forces or DNA-mediated interactions) generally either have no mobility (glass like) or are fully dispersed (plasma like). The rearrangement necessary to obtain ICC's requires long-ranged potentials that can be achieved in low-ionic-strength systems.

Yukawa-type potential to describe the pair interaction energy ($U_{12}$) for particles separated by a distance $r$:

$$U_{12}(r) = \frac{1}{4\pi\varepsilon_0\varepsilon_r} Q_1 Q_2 \frac{\exp(-\kappa r)}{r}. \tag{2}$$

Here the representative point charge ($Q_i$), Eq. (3), is defined as the magnitude of the point charge located at the particle center necessary to generate equivalent electrostatic fields (outside the particle) to those from a spherical shell of charge with the same radius as the particle ($a_i$). For clarity, we present the representative point charge in terms of both the total surface charge ($q_i$) and the surface charge density ($\sigma_i$):

$$Q_i = q_i \frac{\exp(\kappa a_i)}{(1+\kappa a_i)} = 4\pi a_i^2 \sigma_i \frac{\exp(\kappa a_i)}{(1+\kappa a_i)}. \tag{3}$$

Other theories of charged-particle interactions in a medium of charged species have been proposed as alternatives to Poisson-Boltzmann theory. For example, Sogami-Ise theory [31] is developed to explain behaviors not explained by traditional DLVO theory, but does not appear to accurately model colloidal interactions [32]. Another example of an alternative model [33] was developed to simulate experimental situations where the particles and ions are of similar size, breaking the assumption of ergodicity necessary in Poisson-Boltzmann theory. We do not utilize these or other alternative approaches in this work mainly because these theories currently lack the volume of experimental confirmation available for DLVO potentials. The Yukawa-type potential has been used since the inception of DLVO theory to successfully describe many aspects of colloidal behavior and is the most suitable of available potentials to describe an ICC system given that the colloids considered here do not violate the approximations of Poisson-Boltzmann theory.

In any colloidal system other short- and long-range interactions may also be present including van der Waals, acid-base, and depletion interactions, as well as gravitational or other imposed fields. We focus on the interactions that lead to attractive electrostatic stabilization of a crystalline array, recognizing that other interactions may modify the results. These interactions can be incorporated into the electrostatic model of ICC stability presented here and experimentally can often be tailored separately from the electrostatic interactions. As one example, the usually attractive van der Waals interactions can be rendered negligible or even repulsive depending on the dielectric response functions of the materials and the solvent [34].

## III. MADELUNG SUMMATION

Using the Yukawa-type potential, we constructed a model based on a Madelung summation [35] to identify conditions of crystalline stability in systems of oppositely charged particles. The Madelung sum gives the electrostatic energy of a crystal, relative to that of an equal number of isolated lowest-energy formula units for that structure type, and by convention, is greater than unity for an electrostatically stable crystal. It is calculated by first summing the interaction potential over all nonequivalent lattice positions. For a two-component system, the energy of one site ($U_1$) is

$$U_1 = \frac{1}{4\pi\varepsilon_r\varepsilon_0}\left(N_1 Q_1 Q_2 \frac{\exp(-\kappa r_1)}{r_1} + N_2 Q_1^2 \frac{\exp(-\kappa r_2)}{r_2} + N_3 Q_1 Q_2 \frac{\exp(-\kappa r_3)}{r_3} + \cdots\right) \tag{4}$$

Here, $N_i$ corresponds to the number of symmetry equivalent particles at each distance ($r_i$). This is then normalized with respect to the individual bond strength, which is simply the nearest-neighbor interaction energy, giving the Madelung sum ($\alpha_1$) for that site:

$$\alpha_1 = N_1 + N_2 \frac{Q_1}{Q_2}\frac{r_1}{r_2}\exp(\kappa r_1 - \kappa r_2) + N_3 \frac{r_1}{r_3}\exp(\kappa r_1 - \kappa r_3) + \cdots. \tag{5}$$

Equation (5) can be rewritten in terms of two dimensionless parameters with simple physical meanings, a representative point-charge ratio ($Q$) and a screening ratio ($\Lambda$):

$$Q = -\frac{a_1^2\sigma_1 \exp(\kappa a_1)(\kappa a_2 + 1)}{a_2^2\sigma_2 \exp(\kappa a_2)(\kappa a_1 + 1)}, \tag{6}$$

$$\Lambda = \kappa r_1 = \kappa(a_1 + a_2). \tag{7}$$

In classical ionic crystals, $Q$ is limited to values resulting from the valence of the constituent ions and the stoichiometry of the compound. However, for ICC's, $Q$ can be a con-

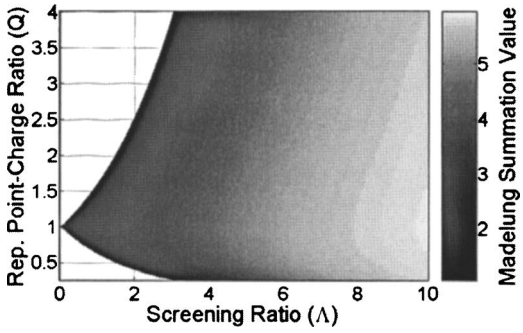


FIG. 2. The Madelung constant for a rocksalt structure is shown as a function of the dimensionless length $\Lambda$ and the representative point charge ratio $Q$. At high values of $\Lambda$, the Madelung constant approaches a maximum value of six (equal to the number of nearest neighbors) corresponding to only nearest-neighbor interactions. At lower values of $\Lambda$ next-nearest-neighbor repulsion becomes more significant, reducing the Madelung sum. The unfilled regions at left have a Madelung constant below one, indicating that this crystal structure is not stable under those conditions. The summation is reciprocally symmetric about $Q=1$ for this structure.

tinuum of charge ratios because the charge on the particles is essentially continuously variable. This allows ICC's to have a nonideal charge ratio for a given structure, while still remaining energetically stable in that structure. The second dimensionless parameter $\Lambda$ gives the spatial extent of the screening relative to the particle radii.

By substituting these dimensionless parameters into Eq. (5), a simplified expression for the Madelung constant is obtained:

$$\alpha_1 = N_1 - N_2 Q \frac{r_1}{r_2} \exp\left(\Lambda - \Lambda \frac{r_2}{r_1}\right) + N_3 \frac{r_1}{r_3} \exp\left(\Lambda - \Lambda \frac{r_3}{r_1}\right) + \cdots . \tag{8}$$

Both the number of particles at each $n$th-nearest-neighbor site and the ratios of the distances, $r_i/r_1$, are characteristic of a given structure and are not variables in the final summation. From Eq. (8) we see that the Madelung "constant" for an ICC system is not a single value, but actually a Madelung surface, varying with the dimensionless parameters $Q$ and $\Lambda$. This surface can be used to determine the experimental conditions under which different ICC structures are stable.

The last step of this Madelung formulation is a weighted summation of the Madelung sum from each nonequivalent lattice site; the number of which is determined by the structure type under consideration. For the rocksalt structure type, there are two nonequivalent sites, the cation and anion sites, which make the first terms of the total Madelung sum ($\alpha_T$):

$$\alpha_T = 6 - 12\left(\frac{Q}{2} + \frac{1}{2Q}\right)\frac{\exp[\Lambda(1-\sqrt{2})]}{\sqrt{2}} + 8\frac{\exp[\Lambda(1-\sqrt{3})]}{\sqrt{3}} - 6\left(\frac{Q}{2} + \frac{1}{2Q}\right)\frac{\exp[\Lambda(1-\sqrt{4})]}{\sqrt{4}} \cdots . \tag{9}$$

Figure 2 shows the Madelung surface for the rocksalt structure as a function of the two dimensionless parameters. Note that although this structure has an ideal representative point-charge ratio of unity, for an ICC deviations from this ideal ratio can still result in a stable crystal ($\alpha > 1$) even though the magnitude of $\alpha$ is not at a maximum for that value of $\Lambda$. At small values of $\Lambda$ (large Debye length), deviations from the ideal charge ratio result in a larger energetic penalty since the solution is less able to screen the imbalance in particle charge. For large $\Lambda$ (small Debye length), particles are highly screened, leaving only nearest-neighbor interactions. Thus, in this limit, the Madelung sum approaches a value equal to the number of nearest neighbors, 6 in the case of the rocksalt structure. As discussed earlier, these next-nearest-neighbor repulsions are important for structural rearrangement, so a Madelung sum near this overall maximum value is nonideal for ICC formation.

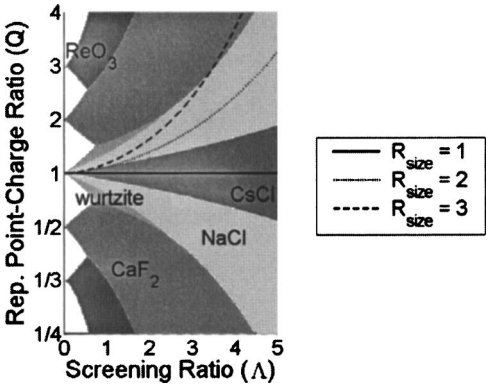


FIG. 3. By comparing the Madelung sum of various structures, a phase stability diagram can be constructed showing the most stable structure of those considered for a given $Q$ and $\Lambda$. While other situations are possible, here a 1:1 number ratio of particles is considered. Various phase fields can be removed via Pauling's rules to give all of the structures accessible at a certain size ratio. For a given system of particles, the relation of $\Lambda$ and $Q$ is given by a monotonic function. Three different size ratios of particles are illustrated here. Movement along a curve is only due to an increase in the ionic strength of the system as all other parameters are held constant. The system becomes more sensitive to changes in ionic strength as the size ratio moves away from unity.

We calculate $\alpha$ for six structure types—rocksalt, zinc blende, wurtzite, cesium chloride, ruthenium oxide, and fluorite—and show their relative stability for a 1:1 number ratio of particles in Fig. 3 (other cases are considered in [18]). Each field identifies the most stable of the six structures (largest value of $\alpha$) in that parameter range. At large values of $\Lambda$, the lowest-energy structure is always that with the most nearest neighbors. At this extreme, the electrostatic interactions are short ranged, leaving little next-nearest-neighbor repulsion. On the other hand, at small values of $\Lambda$, the Yukawa-type potential reduces to Coulomb's law, and as expected, we obtain the established Madelung constants for atomic ionic crystals (e.g., 1.748 for rocksalt, 1.638 for zinc blende, and 1.641 for wurtzite). Other structures not yet evaluated (e.g., rutile, corundum) or defective ICC structures (e.g., with vacancies for charge compensation) may be stable as well. For example, ordered vacancy structures such as bixbyite or pyrochlore could form to compensate non-integer charge ratios.

Pauling's rules provide further criteria for structural stability [36]. For example, following classical arguments, a crystal with a 1:1 stoichometry should favor the cesium chloride structure if the ratio of particle diameters is $<1.366$, the rocksalt structure if the ratio is $<2.415$, and the wurtzite or zinc-blende structures (which are very close in electrostatic energy) if the size ratio lies above 2.415 [37]. A structure with a certain ratio of particle sizes can exhibit a site filling characteristic of a smaller size ratio, but tends not to exhibit one characteristic of a larger size ratio, in which the small ion would not touch all the adjoining nearest neighbors. This would result in a cage of nearest neighbors of the same charged species forced together against large repulsion, while the increased separation between the small ion and its nearest neighbors results in a reduced attractive force. A smaller coordination number may then be energetically favored. Therefore, upon systematically decreasing the size ratio, the rocksalt structure can be made more energetically favorable than cesium chloride (with a critical size ratio of $\geqslant 1.366$) and wurtzite can be stabilized over both (with a critical size ratio of $\geqslant 2.415$). The phase diagram presented in Fig. 3 will then change as the size ratio is varied across a critical size ratio from Pauling's rules and certain structures are eliminated.

The surface charges of particles are typically regulated through materials selection and surface functionalization. Additionally, the absolute and relative particle sizes can be independently controlled. However, once the sizes and surface charge densities for a system of particles are chosen, the energy of the system is constrained to lie along a line given by Eq. (10). As the solution ionic strength is changed, the $Q$ and $\Lambda$ are related by this function, for which examples are given by the curves in Fig. 3 for three size ratios

$$Q(\Lambda) = -R_\sigma R_{size}^2 \frac{1+\Lambda+R_{size}}{(1+\Lambda)R_{size}+1} \exp\left(\Lambda \frac{R_{size}-1}{R_{size}+1}\right)$$
$$= -R_q \frac{1+\Lambda+R_{size}}{(1+\Lambda)R_{size}+1} \exp\left(\Lambda \frac{R_{size}-1}{R_{size}+1}\right). \quad (10)$$

Here, $R_\sigma$ is the ratio of surface charge densities, $R_q$ is the ratio of surface charges, and $R_{size}$ is the ratio of particle sizes, where all ratios are defined for the properties of the large particle over those of the small particle.

The slopes for the three curves in Fig. 3 further illustrate that the sensitivity of $Q(\Lambda)$ to the ionic strength of the solvent depends on the particle size ratio. For size ratios near unity, variations in ionic strength have little effect on the representative point-charge ratio, $Q$. Therefore, the stability of crystals should be tolerant to ionic strength. However, for size ratios far from 1, small changes in ionic strength have a large effect on the representative point-charge ratio.

We envision fabricating ICC's from suspensions containing multiple particle types that are individually nearly monodisperse. The effect of particle size polydispersity on ICC stability is examined using Eq. (10) with the charge density on the particle surface remaining constant with size variations. In Fig. 4, variations on $Q(\Lambda)$ are illustrated for several systems. The illustrated regions of stability are constructed from all possible combinations within one standard deviation

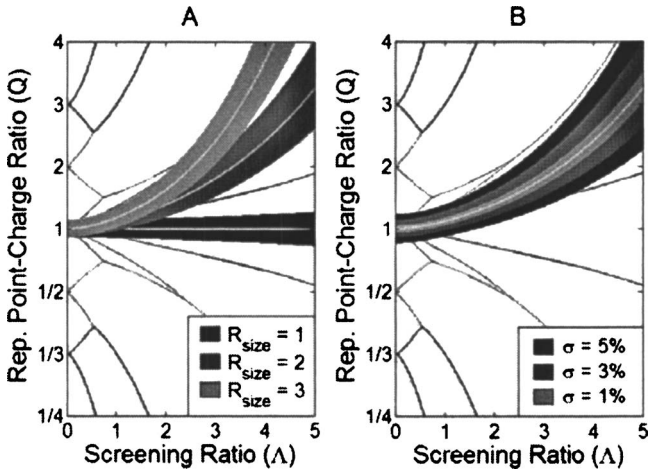


FIG. 4. Several parameters impact the range of representative point-charge ratios present in a system with particle size dispersity. We illustrate the effects of several of these variations for systems with a constant surface charge density. (a) First, we consider the effect on dispersity for systems with $Q(0)=1$, 3% dispersity, and three different size ratios (1, 2, and 3). The shaded regions correspond to the existing charge ratios for all pair combinations within one standard deviation of the central particle sizes. The white lines illustrate the ideal case (i.e., no dispersity) within each region. These variations in charge ratio, which are larger in higher-size-ratio systems, can result in several competing stabilized phases thus frustrating crystallization. The control of screening ratio then becomes even more critical. (b) The impact of various size dispersities is shown for systems of $R_{size}=2$ with 1%, 3%, and 5% dispersity. The large growth in the existing charge ratios with increasing dispersity highlights the necessity of minimizing dispersity as much as possible. Dispersity not only may cause competing phase fields, but may also result in multiple types of site filling by Pauling's rules further increasing the number of competing phases.

of the ideal particle sizes. In Fig. 4(a), the effect of polydispersity on three ideal size ratios is considered. Large size ratios not only cause a sharp increase in the ideal representative point-charge ratio with screening ratio, but also result in a more rapidly broadening range of charge ratios present in the system with increasing screening ratio. These results demonstrate the difficulty in attaining structures with large size ratios (such as wurtzite) over those with near-unity size ratios (such as CsCl). Increased dispersity [as shown in Fig. 4(b)] results in a larger number of competing structures and can possibly result in two different types of site filling as given by Pauling's rules. In both cases, the presence of competing structures will increase the likelihood of frustrated crystallization (glass formation). Therefore, to maximize the likelihood of crystallization, the present results emphasize the need for systems with size distributions narrow enough to not stabilize other phases.

## IV. SIMULATIONS OF ICC FORMATION

While the Madelung summation shows when crystallization is favored over dispersed particle pairs, it does not address the issue of whether crystallization is kinetically favorable over glass formation. Since effective crystallization

requires the tuning of particle interactions to give a melting temperature above and glass transition temperature below the experimental temperature, a computational study of the "melting" behavior of ICCs can provide fundamental insight and guide experiments. We utilized a Monte Carlo approach to calculate the free energy (using the Yukawa potential) of dense disordered heterocoagulates (liquid or glassy state) and an ICC of the rocksalt structure. A constant number, pressure, and temperature (*NPT*) ensemble was utilized at zero pressure. As the pressure exerted by the solution is uniform around the particles and therefore does not change between the various phases, the relevant pressure in calculating the free energy is that exerted by the free colloidal particles in solution, which is usually negligible. For example, the pressure of a dilute (1%) colloidal suspension of 1-$\mu$m particles at 300 K acting as an ideal gas is $8\times10^{-5}$ Pa. In other such cases of low pressure, a zero-pressure assumption has successfully been used to accurately model atomic phase behavior [38]. We modeled a system of particles which based on the Madelung summation is stable in the rocksalt structure type. Conditions giving a value of $\Lambda=3$ were used, and the particle radii and surface charges were chosen to be 1 $\mu$m and 767 positive charges (electron equivalents) for the "cation" and 0.5 $\mu$m and 1389 negative charges for the "anion," giving an actual surface charge ratio of 0.55 and a representative point-charge ratio of 1. The simulated solvent is given the properties of 2-propanol at room temperature.

First, the free volume of the ordered and disordered systems was examined. The free volume of the ordered state smoothly increased with temperature (Fig. 5), while that of the disordered state shows a change in slope at 6950 K, which is indicative of a glass transition. Below the glass transition temperature, each particle can only move within its potential energy well, while above this temperature particle diffusion is activated. For ICC formation, the experimental temperature must lie above the glass transition point.

For both ordered and disordered systems, the internal energy of the system (the sum of all particle interactions) was obtained over a wide range of temperatures. A fit of this data to Eq. (11) was used to calculate the entropy. The free energy of each phase is then given by Eq. (12), where the pressure term is equal to zero (Fig. 6):

$$S=\int_0^{T_1}\frac{C_p}{T}dT=\int_0^{T_1}\frac{\partial H/\partial T|_P}{T}dT, \tag{11}$$

$$G=U+PV-TS=U-TS. \tag{12}$$

Here, $S$ is the system entropy, $C_p$ is the heat capacity of the system, $T_1$ corresponds to the temperature at which the entropy is calculated, $H$ is the system enthalpy, $G$ is the Gibb's free energy of the system, $P$ is the pressure applied by colloids in solution, $V$ is the system volume, and $U$ is the internal energy of the system.

Figure 6 shows an ICC melting point of 7850 K, which is located where the free energies of the disordered heterocoagulate and the ICC cross. The transition temperatures for this system are clearly well above any practical temperature. This system would be greatly undercooled at room temperature, and a glasslike hit-and-stick behavior would be expected due to the absence of colloidal mobility. Indeed, this is the type of behavior normally observed for heterocoagulating colloidal systems. We used these extreme conditions in this example to illustrate a key finding: most heterocoagulating systems will have too high a binding energy to kinetically allow crystallization even when the crystal is energetically the ground state. However, the Monte Carlo simulations are readily rescaled to show when the critical temperatures become practical. In the formulation of Monte Carlo simulations, the interaction energies always appear in conjunction with temperature; therefore, halving the interaction energy will give identical results at half the temperature. Reducing the strength of interactions by reducing the amount of surface charge—i.e., increasing the particle size with a constant amount of surface charge or otherwise reducing the interaction energy—will lead to lower ICC critical temperatures.

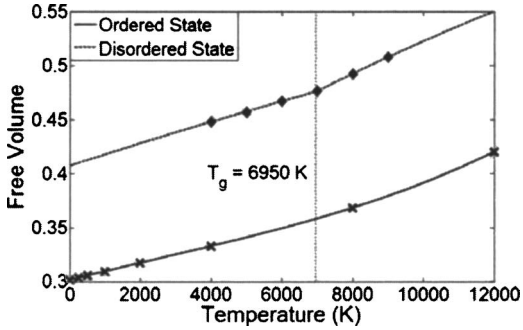


FIG. 5. The free volumes for ordered (ICC) (fit, solid line; data points, ×'s) and disordered states (fit, dashed line; data points, diamonds) are shown as a function of temperature for a system of 1-$\mu$m particles with 767 positive charges (electron equivalents) for the "cation" and 0.5 $\mu$m and 1389 negative charges for the "anion" dispersed in 2-propanol. The free volume of the ordered state increases smoothly, while that of the disordered state shows a distinct discontinuity at 6950 K. This discontinuity is evidence of increased mobility above this temperature. Below this temperature, the structure exhibits a glasslike state with little mobility. The discontinuity is indicative of a glass-transition temperature. For ICC formation to occur, the experimental temperature must be above the glass transition temperature. While the temperatures presented seems impractical, reductions in the particle interactions will result in an equally scaled glass transition temperature. For example, reducing particle interactions from those in the simulated system by a factor of 20 reduces the glass transition temperature to 345 K, a much more accessible temperature.

From the expression for the enthalpy of the system (the bond strength multiplied by the Madelung sum), the melting point ($T_{melt}$) can be expressed as a function of system parameters as follows:

$$T_{melt}=\frac{(-1.44\times10^{21}K/J)\alpha_{total}4\pi a_1^2a_2^2\sigma_1\sigma_2}{\varepsilon_0\varepsilon_r(a_1+a_2)(\kappa a_1+1)(\kappa a_2+1)}$$
$$=\frac{(-1.44\times10^{21}K/J)\alpha_{total}q_1q_2}{4\pi\varepsilon_0\varepsilon_r(a_1+a_2)(\kappa a_1+1)(\kappa a_2+1)}. \tag{13}$$

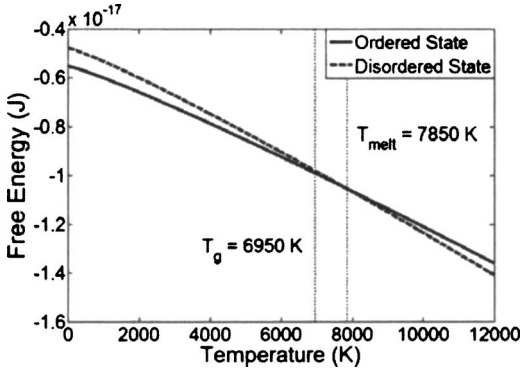


FIG. 6. The free energy as calculated by Monte Carlo simulations is shown for an ordered rocksalt structure (solid line) and a disordered liquid (dashed line) (same system as in Fig. 5). The melting point is found to be 7850 K. This gives a narrow range where crystallization should be possible (between 6950 and 7850 K). The melting point can be reduced by changing the amount of surface charge or the particle sizes to shift this range. Also, by reducing the screening ratio, the accessible region where crystallization can occur should increase. Likewise, increasing the screening ratio results in further convergence of the melting and glass transition temperatures. While these temperatures seem impractical, absolute temperatures can be rescaled with changes in particle interactions. For example, a 20-fold reduction in particle interactions will give glass-transition and melting points of 347 and 392 K, respectively. These results illustrate that for many colloidal systems glass formation may occur even if the lowest-energy state is crystalline.

As an example of the rescaling of temperatures into a practical range, reducing the surface charge densities of both particles in the simulations by a factor of 4.5 while leaving other system parameters unchanged would give a glass transition temperature of 343 K and a melting point of 393 K. This system would then have a particle of 1 $\mu$m radius and 170 positive charges (electron equivalents) for the "cation" and one with a 0.5 $\mu$m radius and 309 negative charges for the "anion." Such an experimental system would have an easily accessible crystallization temperature.

While these results are calculated for a system with $\Lambda = 3$, they give insight into the modifications necessary to obtain crystallization at other values of $\Lambda$. Here, the ratio of the melting point to the glass transition temperature was 0.89. While this is a narrow range, the ratio of the glass transition point to the melting point will be reduced at lower values of $\Lambda$, while the two will converge for higher values of $\Lambda$. Again, this underscores the importance of low-$\Lambda$ systems to ICC formation.

## V. DISCUSSION

We have shown that multiple materials parameters and experimental conditions must be controlled to make an ICC structure thermodynamically and kinetically accessible. It is essential that the particle interaction strength is reduced to give a melting point above and a glass transition temperature below the experimental temperature. The interaction strength can be reduced by reducing the surface charge density at constant particle size or by increasing the particle size for a constant amount of surface charge. Likewise, low values of $\Lambda$ (preferably lower than $\Lambda \sim 3$) must be obtained to allow sufficient mobility for rearrangement. Also, the representative point-charge ratio must be tailored to favor dense crystallization over the agglomeration of isolated particle clusters (preferably $Q$ equal to or lower than 3).

We also note that a system with a glass transition temperature well above the experimental temperature may still crystallize under an external energy source. For example, an ultrasonic source may possibly be used to give the particles sufficient pseudo-Brownian motion to approach a regime where nucleation and growth can occur, providing a larger effective temperature for the system. Other energy sources such as turbulent flow fields and randomly varying ac electric fields may also provide sufficient energy to make crystallization in more systems experimentally accessible.

Higher-order and more complex ICC structures should also be achievable. For example, a similar treatment can be used for structures containing more than two particle types. These could be colloidal analoges of such structures as spinel and perovskite. In addition to ideally nondirectional "ionic" bonding, directional bonding could be introduced using nonspherical particles or anisotropic surface chemistry to synthesize a broader family of colloidal crystals analogous to ionocovalent compounds. An example would be to promote crystallization of zincblende over wurtzite structures. Controlled imperfections (defects and doping) might also be introduced through the addition of small concentrations of particles with sizes or compositions different from those in the bulk of the structure. In addition to accessing a diversity of ordered structures, the rapid formation rate of ICC's under attractive forces suggests that scalable processes could be developed for ICC's. Beyond the formation of basic two-component structures, we believe there are many possible extensions of the ICC concept.

If the concept present in this work is fully realized, there are numerous applications of ICC materials. Ordered colloids of this type could potentially be prepared as pigmentary aggregates, films, or extended three-dimensional crystals. These materials have potential applications including photonics, catalysis, and filtration. Finally, novel mesoscopic materials exhibiting tunable responses to various input fields may also be possible, spawning a new class of device materials.

## VI. CONCLUSIONS

We present a formalism for evaluating the stability of a new class of colloidal crystals that is stabilized by attractive electrostatic interactions. This model allows regions of ICC stability to be described as a function of two dimensionless parameters representing the ratio of particle charges and the spatial extent of the electrostatic interaction, each of which is a function of experimental parameters that are readily

adjusted in colloidal systems. In addition, Monte Carlo calculations have been performed showing the dependence of crystallization and glass transition temperatures in heterocoagulating colloids on these adjustable parameters. Conditions under which ICC's are not only the thermodynamic ground state of the heterocoagulated system, but are also kinetically accessible, are found to be restricted to a rarely explored parameter space in colloidal science, specifically weakly interacting monodisperse heterocoagulating systems at low ionic strength [39].

## ACKNOWLEDGMENTS

The authors acknowledge the financial support of the Deshpande Center for Technological Innovation. G.R. Maskaly thanks the Fannie and John Hertz Foundation for its support. This work was supported by the Chemical Sciences, Biosciences, and Geosciences Division of the Office of Basic Energy Sciences, Office of Science, U.S. Department of Energy, and Los Alamos LDRD Funds.

[1] Y. N. Xia, B. Gates, Y. D. Yin, and Y. Lu, Adv. Mater. (Weinheim, Ger.) **12**, 693 (2000).
[2] A. van Blaaderen, Science **282**, 887 (1998).
[3] A. Stein and R. C. Schroden, Curr. Opin. Solid State Mater. Sci. **5**, 553 (2001).
[4] P. Jiang, J. F. Bertone, K. S. Hwang, and V. L. Colvin, Chem. Mater. **11**, 2132 (1999).
[5] N. Ise, H. Matsuoka, and K. Ito, Angew. Makromol. Chem. **166/167**, 111 (1989).
[6] T. Okubo, Acc. Chem. Res. **21**, 281 (1988).
[7] M. A. Bevan, J. A. Lewis, P. V. Braun, and P. Wiltzius, Langmuir **20**, 7045 (2004).
[8] P. Jiang and M. J. McFarland, J. Am. Chem. Soc. **126**, 13778 (2004).
[9] K. P. Velikov, C. G. Christova, R. P. A. Dullens, and A. van Blaaderen, Science **296**, 106 (2002).
[10] P. Bartlett, R. H. Ottewill, and P. N. Pusey, Phys. Rev. Lett. **68**, 3801 (1992).
[11] P. Bartlett, R. H. Ottewill, and P. N. Pusey, J. Chem. Phys. **93**, 1299 (1990).
[12] P. Bartlett and P. N. Pusey, Physica A **194**, 415 (1993).
[13] A. B. Schofield, Phys. Rev. E **64**, 051403 (2001).
[14] X. Cottin and P. A. Monson, J. Chem. Phys. **102**, 3354 (1995).
[15] N. Hunt, R. Jardine, and P. Bartlett, Phys. Rev. E **62**, 900 (2000).
[16] E. Trizac, M. D. Eldridge, and P. A. Madden, Mol. Phys. **90**, 675 (1997).
[17] S. M. Underwood, W. Vanmegen, and P. N. Pusey, Physica A **221**, 438 (1995).
[18] G. R. Maskaly, Ph.D. Thesis, Massachusetts Institute of Technology, 2005 (http://hdl. handle.net/1721.1/16704).
[19] G. R. Maskaly, R. E. Garcia, W. C. Carter, and Y.-M. Chiang, U.S. Patent Application No. 10/424,672 (2003).
[20] S. Simeonov, U. Bass, and A. R. McGurn, Physica B **228**, 245 (1996).
[21] A. Fernandez-Nieves, J. S. van Duijneveldt, A. Fernandez-Barbero, B. Vincent, and F. J. de las Nieves, Phys. Rev. E **64**, 051603 (2001).
[22] A. Al Sunaidi, M. Lach-hab, A. E. Gonzalez, and E. Blaisten-Barojas, Phys. Rev. E **61**, 550 (2000).
[23] A. Y. Kim and J. C. Berg, J. Colloid Interface Sci. **229**, 607 (2000).
[24] B. V. Derjaguin and L. Landau, Acta Physicochim. URSS **14**, 633 (1941).
[25] E. J. W. Verwey and J. Th. G. Overbeek, *Theory of Stability of Lyophobic Colloids* (Elsevier, Amsterdam, 1948).
[26] R. Hogg, T. W. Healy, and D. W. Fuerstenau, Trans. Faraday Soc. **62**, 1638 (1966).
[27] H. J. Ohshima, J. Colloid Interface Sci. **176**, 7 (1995).
[28] G. R. Wiese and T. W. Healy, Trans. Faraday Soc. **66**, 490 (1970).
[29] B. V. Derjaguin, Kolloid-Z. **69**, 155 (1934).
[30] V. T. Milam, A. L. Hiddessen, J. C. Crocker, D. J. Graves, and D. A. Hammer, Langmuir **19**, 10317 (2003).
[31] I. Sogami and N. Ise, J. Chem. Phys. **81**, 6320 (1984).
[32] J. C. Crocker and D. G. Grier, Phys. Rev. Lett. **77**, 1897 (1996).
[33] J. Z. Wu, D. Bratko, H. W. Blanch, and J. M. Prausnitz, Phys. Rev. E **62**, 5273 (2000).
[34] D. B. Hough and L. R. White, Adv. Colloid Interface Sci. **14**, 3 (1980).
[35] Y.-M. Chiang, D. Birnie, and W. D. Kingery, *Physical Ceramics* (Wiley, New York, 1997), Chap. 1.
[36] L. Pauling, J. Am. Chem. Soc. **51**, 1010 (1929).
[37] When two structures have very similar electrostatic energy, such as wurtzite and zinc blende, the desired structure may be promoted by templating or seeding. The addition of a shaped particle can also make these small changes by adding the colloidal equivalent of covalency.
[38] D. Frenkel and B. Smit, *Understanding Molecular Simulation: From algorithms to applications*, 2nd ed. (Academic Press, San Diego, 2002), Chap. 5.
[39] Recently, experimental evidence of ICC formation was reported in M. E. Leunissen *et al.*, Nature (London) **437**, 235 (2005).